
Novel PET Imaging of Atherosclerosis with ^{68}Ga -Labeled NOTA-Neomannosylated Human Serum Albumin

Eung Ju Kim^{*1}, Sungeun Kim^{*2}, Hong Seog Seo^{1,3}, Yong Jik Lee¹, Jae Seon Eo², Jae Min Jeong⁴, Boeun Lee⁴, Jae Young Kim⁵, Young Mi Park⁶, and Myeongsook Jeong⁶

¹Cardiovascular Center, Korea University Guro Hospital, Korea University College of Medicine, Seoul, South Korea; ²Nuclear Medicine, Korea University Guro Hospital, Korea University College of Medicine, Seoul, South Korea; ³Korea University-Korea Institute of Science and Technology (KU-KIST) Graduate School of Converging Science and Technology, Seoul, South Korea; ⁴Department of Nuclear Medicine, Institute of Radiation Medicine, Seoul National University College of Medicine, Seoul, South Korea; ⁵Research Institute of Skin Imaging, Korea University College of Medicine, Seoul, South Korea; and ⁶Department of Molecular Medicine, Ewha Womans University School of Medicine, Seoul, South Korea

Activated macrophages take up ^{18}F -FDG via glucose transporters, so this compound is useful for atherosclerosis imaging by PET. However, ^{18}F -FDG application is limited for imaging of the heart and brain, in which glucose uptake is high, and in patients with aberrant glucose metabolism. The aims of this study were to confirm that mannosylated human serum albumin (MSA) specifically binds to the mannose receptor (MR) on macrophages and to test the feasibility of ^{68}Ga -labeled NOTA-MSA for PET imaging of atherosclerotic plaques. **Methods:** The peritoneal macrophages of C57/B6 mice were collected, incubated with rhodamine B isothiocyanate-MSA (10 $\mu\text{g}/\text{mL}$), and evaluated by confocal microscopy and flow cytometry. The same evaluations were performed after preincubation of the macrophages with anti-CD206 MR blocking antibodies. NOTA-MSA was synthesized by conjugating 2-(p-isothiocyanatobenzyl)-1,4,7-triazacyclononane-1,4,7-triacetic acid to MSA, followed by labeling with ^{68}Ga . Rabbits with atherosclerotic aorta induced by a 3-mo cholesterol diet and chronic inflammation underwent consecutive PET/CT with ^{18}F -FDG and ^{68}Ga -NOTA-MSA at 2-d intervals. **Results:** The binding of MSA to MR and its dose-dependent reduction by preincubation with anti-CD206 MR blocking antibody were confirmed. Rhodamine B isothiocyanate and fluorescein isothiocyanate fluorescence colocalized at the atherosclerotic plaque. The ^{68}Ga -NOTA-MSA SUVs of the atherosclerotic aorta were significantly higher than those of the healthy arteries and inferior vena cava and were comparable to those obtained with ^{18}F -FDG. **Conclusion:** These findings suggest that MR-specific ^{68}Ga -NOTA-MSA is effective for detecting atherosclerosis in the aorta and is a promising radiopharmaceutical for imaging atherosclerosis because of the presence of M2 macrophages in atherosclerotic plaques.

Key Words: atherosclerosis; inflammation; mannose receptor; positron emission tomography

J Nucl Med 2016; 57:1792–1797

DOI: 10.2967/jnumed.116.172650

Atherosclerosis is the most common underlying pathology in ischemic cardiovascular disease, and its prevalence increases with age, regardless of the presence of risk factors. Although the exact etiology of atherosclerosis is still not known, the characteristic chronic inflammation associated with lipid retention distinguishes it from other inflammatory diseases (1). The inflammatory cells in atherosclerotic lesions are mainly macrophages and T-lymphocytes (1). These macrophages become foam cells through the ingestion of cholesterol in the atherosclerotic plaques.

Despite intensive research efforts in the field of PET, few specific atherosclerosis-targeting agents labeled with positron emitters are available in clinical research. A major advancement in the molecular imaging of atherosclerosis was the development of ^{18}F -FDG, and this metabolic PET reporter agent has been applied to the noninvasive imaging of macrophages in atherosclerotic arteries (2–5). However, the coronary and cerebral arterial segments cannot be evaluated with this method because of the high levels of glucose uptake in the heart (6) and brain (7), and the procedure is also expected to have some limitations in patients with aberrant glucose metabolism (8).

A recent study described PET imaging of atherosclerotic lesions using 2-deoxy-2- ^{18}F -fluoro-D-mannose (^{18}F -FDM) (9). This technique is based on the uptake of mannose by activated macrophages through glucose transporters (GLUTs) (10,11) and the ability of mannose to bind to the mannose receptors (MRs) of macrophages (9). Therefore, because ^{18}F -FDM also targets the MRs on the surface of macrophages, ^{18}F -FDM uptake might be more specific for atherosclerotic plaques than ^{18}F -FDG.

Neomannosylated human serum albumin (MSA) was developed initially for lymphoscintigraphy and imaging of the sentinel lymph nodes (12,13) based on the binding of the terminal mannose residues of MSA to the specific MRs of the lymph nodes. When intravenously injected into rats, mannosylated bovine serum albumin rapidly binds to the Kupffer and endothelial cells in the liver

Received Jan. 14, 2016; revision accepted May 16, 2016.

For correspondence or reprints contact either of the following: Hong Seog Seo, Division of Cardiology, Department of Internal Medicine, Korea University Guro Hospital, 97 Gurodong-gil, Guro-gu, Seoul 152-703, South Korea.

E-mail: mdhsseo@korea.ac.kr

Jae Min Jeong, Department of Biomedical Sciences, Seoul National University College of Medicine, 101 Daehangno, Jongro-gu, Seoul 110-744, South Korea.

E-mail: jmjng@snu.ac.kr

*Contributed equally to this work.

Published online Jun. 23, 2016.

COPYRIGHT © 2016 by the Society of Nuclear Medicine and Molecular Imaging, Inc.

because of the presence of MRs on these cells (14,15). MSA is synthesized by conjugating α -D-mannopyranosylphenyl isothiocyanate (SCN-mannose) with human serum albumin. It was reported that 2-(p-isothiocyanatobenzyl)-1,4,7-triazacyclononane-1,4,7-triacetic acid (SCN-NOTA) is an excellent bifunctional chelating agent for labeling biomolecules with ^{68}Ga (16). Recently, we synthesized ^{68}Ga -labeled MSA with SCN-NOTA for use as a PET probe (17).

Because atherosclerotic lesions contain macrophages that extensively express MRs (18) and NOTA-MSA is not taken up by GLUTs, we postulated that ^{68}Ga -NOTA-MSA would be a novel specific agent for the noninvasive molecular imaging of atherosclerotic lesions by PET. The purpose of this study was to confirm that MSA specifically binds to the MR on macrophages and to evaluate the feasibility of ^{68}Ga -NOTA-MSA compared with that of ^{18}F -FDG for the assessment of advanced atherosclerotic plaques. We used rabbits fed a cholesterol diet and injected with subcutaneous carrageenan to induce systemic inflammation as a model system.

MATERIALS AND METHODS

Preparation of MSA and Rhodamine B (RITC)-Labeled MSA and ^{68}Ga -NOTA-MSA Kit

Methods previously described in the literature were used to synthesize MSA from human serum albumin (13,19), RITC-MSA (15), and NOTA-MSA for ^{68}Ga labeling (17). The labeling efficiency and radiochemical purity determined by instant thin-layer chromatography silica gel were always greater than 98%.

Animal Preparation

Twelve 12-wk-old male New Zealand White rabbits were maintained under standardized conditions (21°C and 41%–62% humidity) with a regular day–night (10–14 h) cycle and free access to water and a laboratory diet. All animal experiments were performed in compliance with the Korea University Animal Science Rules and Regulations and were approved by the Korea University Institutional Animal Care and Use Committee (KUIACUC20110627-1) and the Institutional Animal Care and Use Committee of the Ewha Womans University School of Medicine (ESM-12-0198). The Committee of Animal Experimentation of the Korea University determined that the experimental procedures and housing conditions were compliant with the National Institutes of Health use of laboratory animals or equivalent. The animals were randomly assigned to 1 of 2 groups. The animals in group I ($n = 6$) received a standard chow diet (K-H4 pellets; Ssniff). The animals in group II ($n = 6$) received the same diet as the animals in group I, supplemented with 1.0% (w/w) cholesterol in addition to injections of 0.5 mL of 1% carrageenan subcutaneously every 3 wk to induce systemic inflammation to generate advanced atherosclerotic lesions (20). After 3 mo of treatment, the animals underwent consecutive PET/CT with ^{18}F -FDG and ^{68}Ga -NOTA-MSA at 2-d intervals.

Immunohistochemistry

The mouse monoclonal antirabbit macrophage antibody RAM11 was purchased from Dako/Agilent Technologies (DK-2600). The immunohistochemistry reagents were purchased from Vector Laboratories. The deparaffinized and hydrated slides with xylene and ethanol were reacted with 3% H_2O_2 solution for 10 min, washed, and blocked with normal serum solution for 1 h. The slides were then treated with the primary antibody for 1 h, followed by washing with tris-buffered saline containing 0.05% polysorbate-20. The slides were incubated with secondary antibody for 30 min, washed with tris-buffered saline containing 0.05% polysorbate-20, and treated with the premixed VECTASTAIN ABC (Vector Labs) reagent solution for 30 min. After

being washed and counterstained, the slides were washed with tap water, air-dried, and mounted.

Ex Vivo Study of MSA Binding to MRs of Mouse Macrophages

The antibodies against MR (CD206) and isotype control IgG were purchased from Bio-Rad Laboratories, Inc. The peritoneal macrophages of the C57BL/6 mice ($n = 6$) were collected by peritoneal lavage 4 d after intraperitoneal injection of 4% thioglycolate (1 mL). The mice were euthanized before the macrophages were collected. The cells were cultured in RPMI containing 10% fetal bovine serum. The medium was replaced with serum-free RPMI for the MSA treatment. For the ex vivo study, the macrophages were plated on a coverslip and were incubated with 2 $\mu\text{g}/\text{mL}$ or 10 $\mu\text{g}/\text{mL}$ of the MR-blocking antibody or 10 $\mu\text{g}/\text{mL}$ control immunoglobulin for 90 min at 37°C. The samples were then incubated for 10 min with RITC-MSA (10 $\mu\text{g}/\text{mL}$) and were evaluated using confocal microscopy and flow cytometry.

Examination of Atherosclerotic Lesions in Aorta by Fluorescent Microscopy and Confirmation of Presence of MSA in Lesions

The fluorescent dye, either RITC-MSA (42 $\mu\text{g}/0.1$ mL) or fluorescein isothiocyanate (FITC), was mixed with saline and injected into the rabbit's ear through a vein. These rabbits were sacrificed 10 min thereafter, and the aortas were removed and frozen at -20°C . The dissected aortas were thawed, fixed in 4% (v/v) buffered formalin solution for 30 min, and washed with cold phosphate-buffered saline (pH 7.4). Subsequently, the samples were embedded in optimum-cutting-temperature compound (OCT Compound; Sakura); after incubation, the samples were stored at -80°C for a day to allow dye penetration into the tissues. Sections of 10- μm thickness were cut, placed on poly-D-lysine coated slides, dried at 45°C, and stored at room temperature (protected from light) until use. The tissues were washed twice with phosphate-buffered saline (pH 7.4) to remove the embedding compound and mounted with Fluoromount-G medium (Southern Biotech). The nuclei were labeled with DAPI (4w,6-diaminidino-2-phenylindole; Roche). All stained samples were photographed under a Zeiss microscope equipped with a differential interference contrast cooled camera. The fluorescence images were observed using the IX81-ZDC focus drift compensating microscope (Olympus) with respective excitation and emission wavelengths of 405 and 463 nm for DAPI, 545 and 595 nm for RITC, and 480 and 520 nm for FITC. Fluorescence overlay images were obtained using the Image J program available from the National Institutes of Health.

^{18}F -FDG and ^{68}Ga -NOTA-MSA PET/CT Imaging

The PET/CT procedures were performed using the Gemini TF 16-slice PET/CT scanner (Philips). The TF scanner is a new high-performance, time-of-flight-capable, fully 3-dimensional PET scanner that uses lutetium-yttrium oxyorthosilicate crystals (21). The animals were fasted for at least 12 h before the intravenous injection of ^{18}F -FDG (37.0 MBq/kg) as the positive control probe. The animals were placed in a quiet room for 60 min after anesthesia, and the PET/CT images were obtained thereafter. Two days later, 1 of the hypercholesterolemic rabbits was subjected to ^{68}Ga -NOTA-MSA PET for serial imaging of the atherosclerotic lesions to validate the persistence of the radiopharmaceutical in the atherosclerotic lesions and to determine the clinically relevant duration of atherosclerotic PET imaging, considering the short half-life of ^{68}Ga . After intravenous injection of ^{68}Ga -NOTA-MSA (12.3 MBq/kg), whole-body PET images were acquired (1 min per bed position) at 10, 30, 60, and 120 min after probe injection. After comparison of the serial PET images, the PET images were acquired at 30 min after injection of ^{68}Ga -NOTA-MSA in the other animals.

PET Image Analysis

The PET/CT data acquired in 3 orthogonal planes were displayed on a dedicated workstation (Extended Brilliance Workspace, version 3.5; Philips). The same nuclear medicine physician identified the region of interest on the aortic wall, with its center at the point of local maximum ^{18}F -FDG and ^{68}Ga -NOTA-MSA uptake, throughout the entire study. The maximal SUVs were measured on contiguous axial slices of the thoracic and abdominal aorta, and the mean SUVs of the other organs including the brain, heart, inferior vena cava, liver, spleen, and bone marrow were measured. The SUV is defined as the tissue radioactivity concentration divided by the total injected radioactive substance concentration per body weight. The intra- and interobserver correlation coefficient values of the SUV_{mean} measurements were greater than 0.9.

Statistics

The serum cholesterol level was compared between the control and atherosclerosis groups using the Mann–Whitney U test. The Wilcoxon signed-rank test was used to compare the variables of the ^{18}F -FDG and ^{68}Ga -NOTA-MSA PET/CT findings in the atherosclerosis group. The data were analyzed using SPSS for Windows (version 20.0; SPSS). All statistical results were based on 2-sided tests. A probability value of less than 0.05 was considered statistically significant.

RESULTS

Specific Binding of MSA-RITC to MR on Macrophages Ex Vivo

The binding of MSA-RITC to the specific MRs of the mouse peritoneal macrophages was visualized, and the binding was blocked by preincubation of the macrophages with an MR-blocking antibody (Fig. 1). The flow cytometry findings revealed that the binding of MSA to the MRs decreased in a dose-dependent manner when the macrophages were treated with anti-CD206 MR-blocking antibodies (Supplemental Fig. 1; supplemental materials are available at <http://jnm.snmjournals.org>).

Serum Cholesterol Level Evaluation, Fluorescent Microscopic Examination of Atherosclerotic Aortic Lesions, and Confirmation of Localization of MSA in Atherosclerotic Lesions

The mean serum cholesterol level was 49.01 ± 13.78 mmol/L in the atherosclerotic animals (group II) and 0.96 ± 0.31 mmol/L

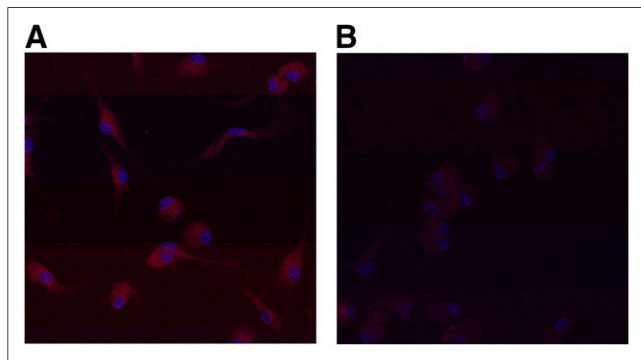


FIGURE 1. Confocal microscopic image showing MR-specific binding of MSA to peritoneal macrophages derived from a C57/BL6 mouse. (A) Macrophages incubated with RITC-MSA and control immunoglobulin, both at concentrations of 10 $\mu\text{g}/\text{mL}$, show red fluorescence. (B) Macrophages preincubated with anti-CD206 MR (10 $\mu\text{g}/\text{mL}$) blocking antibody show markedly diminished fluorescence on incubation with 10 μg of RITC-MSA per mL.

in the control rabbits (group I; $P < 0.001$). In the atherosclerotic aortic lesions (Figs. 2A and 2B; Supplemental Fig. 2), patchy and scattered fluorescent red spots were observed after incubation with RITC-MSA (Fig. 2C); however, the fluorescence on the atherosclerotic plaques with a simple fluorochrome such as FITC was faint (Fig. 2D), indicating that RITC-MSA bound specifically to the MRs (Fig. 2E). The fluorescence on the medial walls of the atherosclerotic (Fig. 2) and healthy aortas (Supplemental Fig. 3) was considered to be due to autofluorescence of the collagen and elastin content in the arterial walls (22).

Findings from ^{18}F -FDG and ^{68}Ga -NOTA-MSA PET Imaging Studies

The persistence of the SUV of the radiotracers was confirmed by the visualization of the atherosclerotic aorta at all time points, and no significant differences were found in the persistence between the 10- and 60-min postinjection images of the atherosclerotic aorta (Fig. 3). Therefore, we decided to acquire the PET images 30 min after the injection of the radiotracers in the animals. The ^{18}F -FDG and ^{68}Ga -NOTA-MSA SUVs of the internal organs in the control and atherosclerotic rabbits are presented in Supplemental Table 1 and Supplemental Figure 4. Compared with the control animals, the atherosclerotic animals showed higher ^{68}Ga -NOTA-MSA uptake in the aorta in the ^{68}Ga -NOTA-MSA PET images and higher ^{18}F -FDG uptake in the ^{18}F -FDG PET images (Figs. 4A and 4B; Supplemental Fig. 5). In the atherosclerotic aorta, the maximal SUVs of ^{68}Ga -NOTA-MSA were higher than those of ^{18}F -FDG (Figs. 5A and 5B), but the SUV ratio of the aorta to the inferior vena cava was not different between the 2 probes (abdominal aorta, $P = 0.432$; thoracic aorta, $P = 0.368$) (Fig. 5C; Supplemental Table 1).

DISCUSSION

In this study, we confirmed that MSA specifically binds to the MRs on macrophages and that ^{68}Ga -NOTA-MSA is a feasible molecular imaging PET probe for atherosclerotic lesions in rabbits. The SUVs of the aorta and the ratio of the SUV of the aorta to that of the inferior vena cava with ^{68}Ga -NOTA-MSA PET/CT imaging were higher in the atherosclerotic animals than in the control animals and were not different from those obtained with ^{18}F -FDG PET/CT imaging. These findings suggest that ^{68}Ga -NOTA-MSA could be a promising radiopharmaceutical agent for the detection and imaging of atherosclerosis by detecting the MR activity of macrophages in atherosclerotic plaques.

Currently, no atherosclerosis-specific targeting agent labeled with a positron emitter is available for clinical research. Rudd et al. imaged atherosclerotic plaques by assessing the ^{18}F -FDG uptake of macrophages based on the metabolic characteristics of the inflammatory cells (2–4). On the basis of the results of these studies, the metabolic PET reporter agent ^{18}F -FDG is currently considered the standard agent for imaging atherosclerotic plaques. Additionally, Tawakol et al. quantified inflammation in the carotid plaques using in vivo ^{18}F -FDG PET imaging (5).

However, the metabolic characteristics of ^{18}F -FDG are responsible for its limited usefulness for atherosclerotic imaging in patients with conditions related to abnormal glucose metabolism, such as diabetes (8), and in organs that use glucose as the main source of energy, including the heart and brain (7,8). Therefore, the coronary and cerebral arterial segments are currently

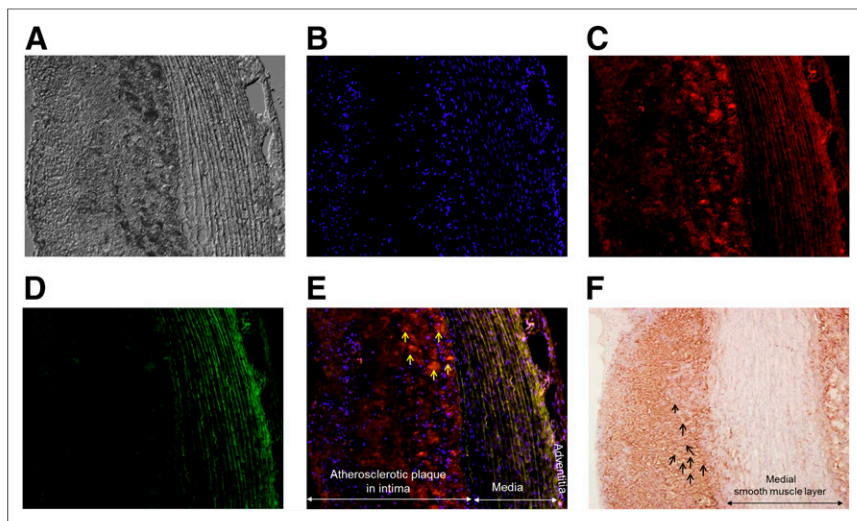


FIGURE 2. Representative images illustrating RITC-MSA binding to MRs in aortic plaque of atherosclerotic rabbit. (A) Differential interference contrast microscopy image of an atherosclerotic plaque in the rabbit aorta. (B) DAPI-stained nuclei (blue) visualized in the same fields by switching to fluorescence confocal microscopy. (C) Red fluorescent image of same atherosclerotic plaque and medial layers of aorta after incubation with RITC-MSA. (D) IX81-ZDC focus drift-compensating microscope showing faint green fluorescence of FITC over atherosclerotic lesion, with definite fluorescence over medial smooth muscle layers (excitation and emission wavelengths of 480 and 520 nm for FITC and 545 and 595 nm for RITC, respectively). (E) Overlay of fluorescent images of atherosclerotic aorta, with yellow arrows indicating presence of M2 macrophages. (F) Immunohistochemistry photograph (magnification, 100x) of aortic atherosclerotic lesion labeled with antirabbit macrophage monoclonal antibody RAM11 at adjacent portion of aorta shown in representative fluorescence images. Arrows indicate presence of macrophages. Presence of lipid-laden macrophages in atherosclerotic rabbit is demonstrated in Supplemental Figure 2.

uninterpretable with ^{18}F -FDG (6), and these limitations of ^{18}F -FDG for imaging of atherosclerosis remain unresolved. A recent study reported PET imaging of atherosclerosis in rabbits with ^{18}F -FDM (9). However, atherosclerotic imaging with ^{18}F -FDM is not entirely specific to the MRs because mannose is a sugar monomer

phenotype by varying the expression of receptors, depending on the stage of inflammation and the microenvironment of the inflammatory lesions (25). M2-subtype macrophages express MRs related to homeostasis, angiogenesis, tissue repair, and fibrosis in the local inflammatory lesion (26). Therefore, M2 macrophages might inhibit inflammation and prevent plaque rupture

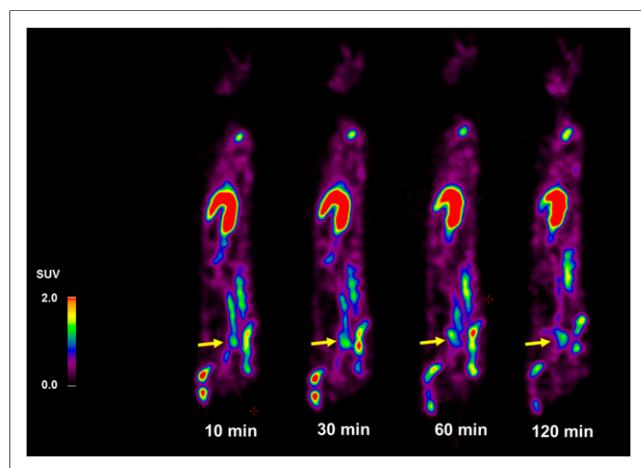


FIGURE 3. Sequential ^{68}Ga -NOTA-MSA PET images of atherosclerosis at 10, 30, 60, and 120 min after tracer injection confirm persistence of radiopharmaceutical by visualization of atherosclerotic aorta (yellow arrow) until 120 min in cholesterol-fed atherosclerotic rabbit. Maximal SUVs of atherosclerotic aorta at 10, 30, 60, and 120 min were 1.7, 1.8, 1.5, and 1.2, respectively. Liver and bone marrows of spine, pelvis, and femur also showed high uptake of ^{68}Ga -NOTA-MSA, indicating intensity of cells presenting MRs in reticuloendothelial system (17).

($\text{C}_6\text{H}_{12}\text{O}_6$) of a small molecule, and the atherosclerotic lesions are labeled by means of enhanced uptake by activated macrophages via GLUTs and by the agent binding to macrophage MRs (9). To overcome the limitations of ^{18}F -FDG and ^{18}F -FDM imposed by metabolic processes and to achieve atherosclerotic imaging that is more specific for MRs, we developed NOTA-MSA, a macromolecule that cannot be taken up by GLUTs but can rapidly bind to the MRs on macrophages (17). In our ex vivo study, we confirmed that the use of an MR-blocking antibody inhibited the binding of MSA to the macrophages. The visualization of atherosclerotic lesions in the ^{68}Ga -NOTA-MSA PET images was persistent. Theoretically, in contrast to ^{18}F -FDG imaging, the assessment of atherosclerosis with ^{68}Ga -NOTA-MSA would be possible even in cases of aberrant glucose metabolism. These results indicate that MR-specific ^{68}Ga -NOTA-MSA could be used extensively for the detection of atherosclerosis, regardless of the patients' metabolic conditions.

Recently, reports indicate that radioisotope-labeled nanoparticles including core-free dextran nanoparticles allow macrophage detection in atherosclerotic plaques in PET imaging (23,24). Macrophages can change

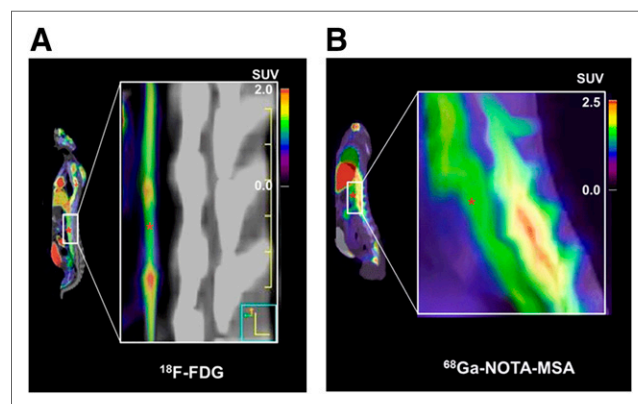


FIGURE 4. Representative examples of ^{18}F -FDG and ^{68}Ga -NOTA-MSA PET images in atherosclerotic rabbit fed cholesterol diet. Comparison of ^{18}F -FDG and ^{68}Ga -NOTA-MSA PET images of atherosclerotic aorta reveals visualization of aortic lesions with both tracers. Magnified uptake of ^{18}F -FDG at 60 min after injection (A) and ^{68}Ga -NOTA-MSA at 30 min after injection at abdominal aorta (red asterisks) (B). Vertebral column is visible in enlarged PET/CT images. PET images were acquired 60 min after intravenous injection of ^{18}F -FDG and 30 min after injection of ^{68}Ga -NOTA-MSA.

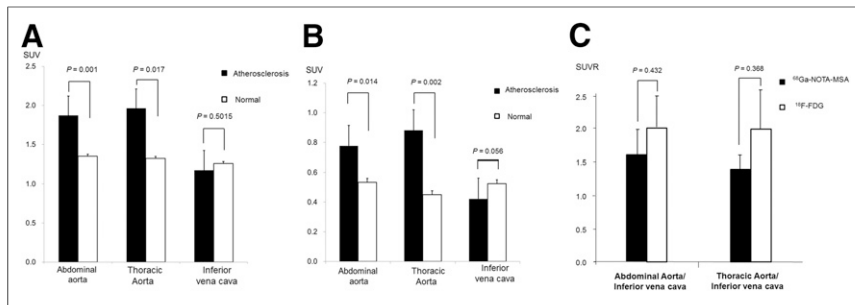


FIGURE 5. SUVs of atherosclerotic lesions and normal aorta with ^{68}Ga -MSA (A) and ^{18}F -FDG (B) and SUV ratio (SUVR) of atherosclerotic aorta to inferior vena cava (C) in PET images. Maximal SUVs were measured at aorta and mean SUVs at inferior vena cava. Maximal SUVs of ^{68}Ga -NOTA-MSA were higher than those of ^{18}F -FDG (A and B) in atherosclerotic aorta, but SUVR of aorta to inferior vena cava was not significantly different between ^{18}F -FDG and ^{68}Ga -NOTA-MSA images (C).

in atherosclerotic lesions (18). However, the role of M2 macrophages in atherosclerosis has not yet been clarified. A recent quantitative evaluation of the macrophages in human plaques revealed a significantly higher density of M2 and MR-bearing macrophages in the high-risk plaques obtained from subjects who had experienced sudden cardiac death (9). Given that MSA is a specific ligand of the MRs of macrophages (15), ^{68}Ga -NOTA-MSA-mediated imaging of atherosclerosis can be considered more specific for the pure, MR-bearing macrophages in the vulnerable atherosclerotic lesions, whereas the subtypes of the macrophages in atherosclerotic plaques could not be determined using PET imaging with dextran nanoparticles (23,24). In addition to plaque characterization, ^{68}Ga -NOTA-MSA might be able to detect atherosclerotic plaques even in the cerebral arteries, because the large size of the albumin molecule of MSA does not allow it to cross the blood-brain barrier.

It is difficult to understand how this macromolecule penetrates the arterial wall to result in adequate labeling of the atherosclerotic plaques for PET imaging. According to a small-animal PET biodistribution study performed after intravenous injection in normal mice, the accumulation of ^{68}Ga -NOTA-MSA in the organs of the reticular endothelial system, such as the liver, spleen, and bone marrow, remained almost constant from 10 min until 2 h after injection, at which point bladder uptake was observed (17). Preinjection of MSA as a blocking agent resulted in decreased uptake of ^{68}Ga -NOTA-MSA in the liver and spleen, indicating specific uptake by MRs in these organs (17). The rapid reticular endothelial system uptake of ^{68}Ga -NOTA-MSA would result in background clearance, enabling excellent contrast for macrophage imaging when its uptake occurs in the vascular compartment. MSA is not visible at the vascular tree, including the aorta, when injected intravenously in normal animals because of its large molecular size (17). However, the permeability around the endothelia that has been damaged by vascular inflammation at the atherosclerotic plaques is high enough for albumin to diffuse into the vessel wall (27). Further, we confirmed the persistence of ^{68}Ga -NOTA-MSA at the atherosclerotic aorta from 10 to 120 min after injection. This finding suggests that ^{68}Ga -NOTA-MSA diffuses into atherosclerotic plaques at an early point and that ^{68}Ga -NOTA-MSA binds to the MRs of atherosclerotic lesions.

In this study, we used the ^{68}Ga isotope for PET. ^{68}Ga is known to be a convenient and economical positron emitter (28,29). ^{68}Ga

(β^+ emission, 89%; half-life, 67.6 min) is an emerging radioisotope for PET because of its wide availability with the easy-to-use and economic $^{68}\text{Ge}/^{68}\text{Ga}$ generator (29). In general, ^{18}F labeling requires a considerable preparation time before injection because of processes such as cyclotron operation, water and solvent evaporation, and radiolabeling for at least 1–2 h. However, ^{68}Ga labeling requires only 20 min of preparation time for the generator elution and radiolabeling steps (17). Moreover, ^{68}Ga has the advantage of radiolabeling without the necessity of an expensive cyclotron (28,29), and ^{68}Ga -labeling kits to prepare ^{68}Ga -NOTA-MSA can be formulated to further simplify the labeling procedure (17). Therefore, the use

of ^{68}Ga -NOTA-MSA for atherosclerosis imaging shows promise for clinical applications.

CONCLUSION

Macrophage MR-specific ^{68}Ga -NOTA-MSA can detect atherosclerotic lesions and could be a promising PET agent for the molecular imaging of the atherosclerotic plaque burden.

DISCLOSURE

The costs of publication of this article were defrayed in part by the payment of page charges. Therefore, and solely to indicate this fact, this article is hereby marked “advertisement” in accordance with 18 USC section 1734. This study was partly supported by grants from the Korea Institute of Science and Technology Institutional Program (project no. 2E24080); Korea University-Korea Institute of Science and Technology (KU-KIST) Graduate School of Converging Science and Technology (R1307922); and the Korea Health Industry Development Institute (KHIDI), funded by the Ministry of Health & Welfare, Republic of Korea (HI15C3093). No other potential conflict of interest relevant to this article was reported.

REFERENCES

- Ross R. Atherosclerosis: an inflammatory disease. *N Engl J Med*. 1999;340:115–126.
- Rudd JH, Warburton EA, Fryer TD, et al. Imaging atherosclerotic plaque inflammation with [^{18}F]-fluorodeoxyglucose positron emission tomography. *Circulation*. 2002;105:2708–2711.
- Rudd JH, Myers KS, Bansilal S, et al. Atherosclerosis inflammation imaging with ^{18}F -FDG PET: carotid, iliac, and femoral uptake reproducibility, quantification methods, and recommendations. *J Nucl Med*. 2008;49:871–878.
- Rudd JH, Myers KS, Bansilal S, et al. ^{18}F Fluorodeoxyglucose positron emission tomography imaging of atherosclerotic plaque inflammation is highly reproducible: implications for atherosclerosis therapy trials. *J Am Coll Cardiol*. 2007;50:892–896.
- Tawakol A, Migrino RQ, Bashian GG, et al. In vivo ^{18}F -fluorodeoxyglucose positron emission tomography imaging provides a noninvasive measure of carotid plaque inflammation in patients. *J Am Coll Cardiol*. 2006;48:1818–1824.
- Mabuchi M, Kubo N, Morita K, et al. Value and limitation of myocardial fluorodeoxyglucose single photon emission computed tomography using ultra-high energy collimators for assessing myocardial viability. *Nucl Med Commun*. 2002;23:879–885.

7. Gjedde A. Does deoxyglucose uptake in the brain reflect energy metabolism? *Biochem Pharmacol.* 1987;36:1853–1861.
8. Voipio-Pulkki LM, Nuutila P, Knuuti MJ, et al. Heart and skeletal muscle glucose disposal in type 2 diabetic patients as determined by positron emission tomography. *J Nucl Med.* 1993;34:2064–2067.
9. Tahara N, Mukherjee J, de Haas HJ, et al. 2-deoxy-2-[¹⁸F]fluoro-D-mannose positron emission tomography imaging in atherosclerosis. *Nat Med.* 2014;20:215–219.
10. Gould GW, Thomas HM, Jess TJ, Bell GI. Expression of human glucose transporters in *Xenopus* oocytes: kinetic characterization and substrate specificities of the erythrocyte, liver, and brain isoforms. *Biochemistry.* 1991;30:5139–5145.
11. Shepherd PR, Kahn BB. Glucose transporters and insulin action: implications for insulin resistance and diabetes mellitus. *N Engl J Med.* 1999;341:248–257.
12. Takagi K, Uehara T, Kaneko E, et al. ^{99m}Tc-labeled mannosyl-neoglycoalbumin for sentinel lymph node identification. *Nucl Med Biol.* 2004;31:893–900.
13. Jeong JM, Hong MK, Kim YJ, et al. Development of ^{99m}Tc-neomannosyl human serum albumin (^{99m}Tc-MSA) as a novel receptor binding agent for sentinel lymph node imaging. *Nucl Med Commun.* 2004;25:1211–1217.
14. Ogawara K, Hasegawa S, Nishikawa M, Takakura Y, Hashida M. Pharmacokinetic evaluation of mannosylated bovine serum albumin as a liver cell-specific carrier: quantitative comparison with other hepatotropic ligands. *J Drug Target.* 1999;6:349–360.
15. Kim S, Jeong JM, Hong MK, et al. Differential receptor targeting of liver cells using ^{99m}Tc-neoglycosylated human serum albumins. *Arch Pharm Res.* 2008;31:60–66.
16. Jeong JM, Hong MK, Chang YS, et al. Preparation of a promising angiogenesis PET imaging agent: ⁶⁸Ga-labeled c(RGDyK)-isothiocyanatobenzyl-1,4,7-triazacyclononane-1,4,7-triacetic acid and feasibility studies in mice. *J Nucl Med.* 2008;49:830–836.
17. Choi JY, Jeong JM, Yoo BC, et al. Development of ⁶⁸Ga-labeled mannosylated human serum albumin (MSA) as a lymph node imaging agent for positron emission tomography. *Nucl Med Biol.* 2011;38:371–379.
18. Mantovani A, Garlanda C, Locati M. Macrophage diversity and polarization in atherosclerosis: a question of balance. *Arterioscler Thromb Vasc Biol.* 2009;29:1419–1423.
19. Kim HK, Kim S, Sung HK, Lee YS, Jeong JM, Choi YH. Comparison between preoperative versus intraoperative injection of technetium-99 m neomannosyl human serum albumin for sentinel lymph node identification in early stage lung cancer. *Ann Surg Oncol.* 2012;19:1343–1349.
20. Kim EJ, Kim BH, Seo HS, et al. Cholesterol-induced non-alcoholic fatty liver disease and atherosclerosis aggravated by systemic inflammation. *PLoS One.* 2014;9:e97841.
21. Surti S, Kuhn A, Werner ME, Perkins AE, Kolthammer J, Karp JS. Performance of Philips Gemini TF PET/CT scanner with special consideration for its time-of-flight imaging capabilities. *J Nucl Med.* 2007;48:471–480.
22. Monici M. Cell and tissue autofluorescence research and diagnostic applications. *Biotechnol Annu Rev.* 2005;11:227–256.
23. Majmudar MD, Yoo J, Keliher EJ, et al. Polymeric nanoparticle PET/MR imaging allows macrophage detection in atherosclerotic plaques. *Circ Res.* 2013;112:755–761.
24. Nahrendorf M, Zhang H, Hembrador S, et al. Nanoparticle PET-CT imaging of macrophages in inflammatory atherosclerosis. *Circulation.* 2008;117:379–387.
25. Stout RD, Jiang C, Matta B, Tietzel I, Watkins SK, Suttles J. Macrophages sequentially change their functional phenotype in response to changes in micro-environmental influences. *J Immunol.* 2005;175:342–349.
26. Taylor PR, Martinez-Pomares L, Stacey M, Lin HH, Brown GD, Gordon S. Macrophage receptors and immune recognition. *Annu Rev Immunol.* 2005;23:901–944.
27. Phinikaridou A, Andia ME, Protti A, et al. Noninvasive magnetic resonance imaging evaluation of endothelial permeability in murine atherosclerosis using an albumin-binding contrast agent. *Circulation.* 2012;126:707–719.
28. Ehrhardt GJ, Welch MJ. A new germanium-63/gallium-68 generator. *J Nucl Med.* 1978;19:925–929.
29. Zhernosekov KP, Filosofov DV, Baum RP, et al. Processing of generator-produced ⁶⁸Ga for medical application. *J Nucl Med.* 2007;48:1741–1748.